

# Interaction between fluids and Helfrich membranes

Michele Castellana<sup>1,2</sup>

<sup>1</sup>*Institut Curie, PSL Research University, Paris, France*

<sup>2</sup>*CNRS UMR168, 11 rue Pierre et Marie Curie, 75005, Paris, France*

(Dated: January 8, 2026)

1. [1] study the steady state with arc-length gauge
2. In the dynamics, arc-length gauge does not work
3. We show how to use a generalized arc-length gauge and how to correctly incorporate it into the dynamics to obtain a proper dynamics, Fig. 6.
4. In this dynamics
  - we implement the Crank-Nicolson method to the equations written in the reference configuration, and prove it to be numerically stable
  - we show that the derivative of mesh motion  $\dot{\mathbf{u}}_D$  can be obtained exactly from an auxiliary PDE without recurring to error-prone time discretization.
5. We couple the membrane dynamics to a bulk fluid. The membrane is a complex elastic body -i. We proceed by steps:
  - (a) Bulk fluid + rigid body Fig. 2
  - (b) Elastic body with stable elastic model (stable under compression)
  - (c) Bulk fluid + elastic body with stable elastic model, Fig. 5
  - (d) Bulk fluid + membrane, Fig. 7
    - Bulk fluid and membrane both described with Crank-Nicolson method -i. we prove that the resulting dynamics is numerically stable. Say that you found a way to replace  $t \rightarrow t_n$  that is stable and that you could have used other ways which are also correct to within  $\mathcal{O}(\Delta t)$ .
    - It allows for overhangs
    - It is the first study that describes a bulk fluid coupled to a Helfrich membrane with ALE

- It allows for turbulent behavior for both the bulk fluid and the membrane tangential flow

## Perspectives:

1. Study nucleoid compaction in E. Coli with ALE

## I. FLUID AND RIGID BODY

In this Section, we will discuss the interaction between a **bulk fluid** (**F**) and the simplest structure—a **rigid body** (**R**) which is only allowed to turn about one point.

In all the systems that we will consider, we will introduce the **reference** (**r**) and **current** (**c**) configuration [2–4], see Fig. 1. All quantities relative to the **r** and **c** configuration will be denoted by the superscript **r** and **c**, respectively. In the **r** configuration, the region occupied by the bulk fluid is described by Cartesian coordinates  $\mathbf{x}_r$ . The axis of the ellipse, e.g., the rigid body, lies parallel to the  $x_c^1$  axis. In the **c** configuration, the region occupied by the bulk fluid is described by Cartesian coordinates  $\mathbf{x}_c$ . The axis of the ellipse, e.g., the rigid body, forms an angle  $\theta$  (red arc) with respect to the  $x_c^1$  axis.

The **r** configuration, is related to the **c** one as follows [2], see Fig. 1. At time  $t$ , the point  $\mathbf{x}_c$  corresponds to a point  $\mathbf{x}_r$  in the reference configuration through the deformation field [5]

$$\mathbf{u}_D^t(\mathbf{x}_r) \equiv \mathbf{x}_c - \mathbf{x}_r. \quad (1)$$

and the deformation-gradient tensor

$$F_{\alpha\beta}(\mathbf{u}) \equiv \delta_{\alpha\beta} + \frac{\partial u^\alpha}{\partial x_r^\beta}, \quad (2)$$

read [6]

where we set

$$\partial_{\alpha}^r \equiv \frac{\partial}{\partial x_r^{\alpha}}, \quad (3)$$

$$\partial_{\alpha}^c \equiv \frac{\partial}{\partial x_c^{\alpha}}. \quad (4)$$

Here, we will denote the mapping between  $\mathbf{x}_c$  and  $\mathbf{x}_r$  in Eq. (1) with the fields

$$\mathbf{x}_c = \varphi^t(\mathbf{x}_r), \quad (5)$$

$$\mathbf{x}_r = \psi^t(\mathbf{x}_c). \quad (6)$$

We denote the  $\mathbf{F}$  velocity and surface tension by  $v_c(\mathbf{x}_c)$  and  $\sigma_c(\mathbf{x}_c)$ , respectively, where the superscript  $c$  specifies that these fields depend on the coordinate  $\mathbf{x}_c$  in the  $c$  configuration.

The solution of the interaction dynamics between  $\mathbf{F}$  and  $\mathbf{R}$  is involved because of the presence of the moving boundary  $\partial\Omega_c^c$ , cf. Fig. 1. Following the arbitrary Lagrangian-Eulerian (ALE) procedure, we will bridge between the Lagrangian and the Eulerian description used to describe, respectively,  $\mathbf{R}$  and  $\mathbf{F}$  [2]. To achieve this, in what follows we will write the equations of motion for  $\mathbf{R}$  and  $\mathbf{F}$ , which are naturally formulated the  $c$  configuration first, and then rewrite them in the  $r$  configuration.

### A. Rigid body motion

In this Section, we will work out the equations of motion for  $\mathbf{R}$ .

#### 1. Equation of motion in the *current*-configuration coordinates

The dynamics of  $\mathbf{R}$  is given by the equations of motion for a rigid body which, in  $c$  coordinates,

Equation (7) relates the angular acceleration of  $\mathbf{R}$  to the torque of external forces. In what follows, Greek indices  $\alpha, \beta, \dots$  will be used to denote vectors and tensors in two-dimensional Euclidean space—their

position as upper or lower indices is thus immaterial [3, 7]. The moment of inertia of  $\mathbf{R}$  is denoted by  $I$ . The right-hand side (RHS) of Eq. (7) contains the line integral along the boundary of  $\mathbf{R}$ , of the torque of the local force exerted by  $\mathbf{F}$  on  $\mathbf{R}$  with respect to the left focal point  $\mathbf{f}$  of  $\mathbf{R}$  [5]. This force is expressed in terms of the  $\mathbf{F}$  stress tensor [5]

$$\varsigma^c_{\alpha\beta} \equiv \sigma_c \delta_{\alpha\beta} + \eta_F \left( \frac{\partial v_c^\alpha}{\partial x_c^\beta} + \frac{\partial v_c^\beta}{\partial x_c^\alpha} \right), \quad (9)$$

where  $\epsilon_{\alpha\beta\gamma}$  is the three-dimensional Levi-Civita symbol, and  $\eta_F$  the two-dimensional viscosity of  $\mathbf{F}$ . Finally,  $dl_c$  is the line element of  $\partial\Omega_c^c$  in the  $c$  configuration, and  $\hat{\mathbf{n}}^c$  the unit boundary normal to  $\partial\Omega_c^c$  pointing outside  $\Omega^c$ .

#### 2. Equation of motion in the *reference*-configuration coordinates

---


$$I \frac{d\omega}{dt} = \int_{\partial\Omega_c^r} ds \epsilon_{\alpha\beta} [\varphi^{\alpha,t}(\xi(s)) - f^\alpha] \varsigma^r_{\beta\gamma}(\xi(s)) \epsilon_{\gamma\lambda} F_{\lambda\mu}(\mathbf{u}_D^t(\xi(s))) \frac{d\xi^\mu(s)}{ds} \quad (10)$$


---

In Eq. (10), the integral in the RHS is over the

curvilinear boundary  $\partial\Omega_c^r$ , which is parametrized

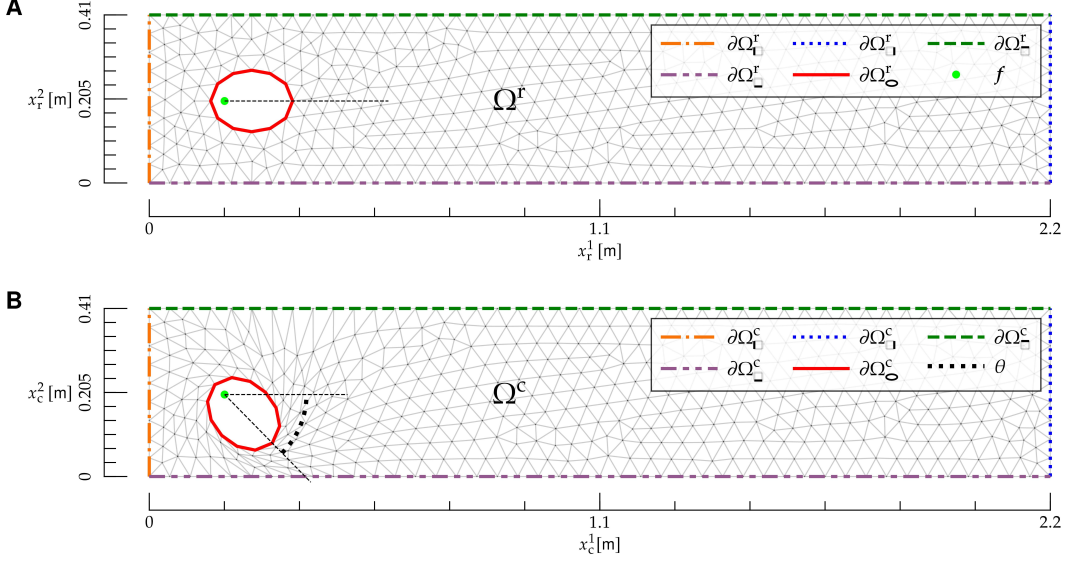


**FIG. 1:** Reference and current configuration for the interaction between a bulk fluid and a rigid body. **A)** Reference configuration. The region  $\Omega^r$  is given by the rectangle  $0 \leq x_r^1 \leq L$ ,  $0 \leq x_r^2 \leq h$  with the elliptical hole, and is delimited by the mesh (gray lines). Boundaries in the reference configuration are denoted by  $\partial\Omega_{\square}^r$ ,  $\partial\Omega_{\square}^r$ ,  $\partial\Omega_{\square}^r$  and  $\partial\Omega_{\square}^r$  (colored dashed lines). The ellipse focal point  $f$  (light green dot) is also shown. **B)** Current configuration. The region  $\Omega^c$  is delimited by the mesh (gray lines). Boundaries in the current configuration are denoted by  $\partial\Omega_{\square}^c$ ,  $\partial\Omega_{\square}^c$ ,  $\partial\Omega_{\square}^c$ ,  $\partial\Omega_{\square}^c$  and  $\partial\Omega_{\square}^c$  (colored dashed lines), and the rotational angle  $\theta$  of the rigid body is shown as an arc (black dotted line). The Cartesian coordinates  $\mathbf{x}_c$  are also shown.

as  $\mathbf{x}_r = \xi(s)$ , where  $s$  is the curvilinear coordinate. Also,  $\epsilon_{\alpha\beta}$  is the two-dimensional Levi-Civita symbol [7], and  $\varsigma^r$  denotes the stress tensor in the  $r$  configuration:

$$\begin{aligned} \varsigma^{rt}_{\alpha\beta}(\mathbf{x}_r) &\equiv \varsigma^c_{\alpha\beta}(\varphi^t(\mathbf{x}_r)) \\ &= \sigma_r(\mathbf{x}_r, t)\delta_{\alpha\beta} + \eta_F \left[ G_{\gamma\beta}(\mathbf{u}_D^t(\mathbf{x}_r)) \frac{\partial v_c^\alpha}{\partial x_r^\gamma} + \right. \\ &\quad \left. G_{\gamma\alpha}(\mathbf{u}_D^t(\mathbf{x}_r)) \frac{\partial v_c^\beta}{\partial x_r^\gamma} \right], \end{aligned} \quad (11)$$

where

$$G_{\alpha\beta}(\mathbf{u}) \equiv [F(\mathbf{u})]_{\alpha\beta}^{-1}. \quad (12)$$

## B. Fluid motion

In this Section, we will work out the equations of motion for  $\mathbf{F}$ .

### 1. Equations of motion in the current-configuration coordinates

The equations of motion, expressed in terms of the  $c$  fields  $v_c$  and  $\sigma_c$ , are

$$\rho_F \left( \partial_t v_c^\alpha + v_c^\beta \frac{\partial v_c^\alpha}{\partial x_c^\beta} \right) = \frac{\partial \sigma_c}{\partial x_c^\alpha} + \eta_F \frac{\partial}{\partial x_c^\beta} \frac{\partial v_c^\alpha}{\partial x_c^\beta}, \quad (13)$$

$$\frac{\partial v_c^\alpha}{\partial x_c^\alpha} = 0, \quad (14)$$

and they hold for  $x_c \in \Omega^c$ . Equations (13) and (14) are the Navier-Stokes (NS) and continuity equation, respectively, in a flat, two-dimensional geometry [5]—an example of the NS equations on curved geometry will be presented in X. There,  $\rho_F$  is the two-dimensional  $F$  density.

The boundary conditions (BCs) for Eqs. (7), (8), (13) and (14) are

$$v_c^1(\mathbf{x}_c) = v_* \text{ on } \partial\Omega_{\square}^c, \quad (15)$$

$$v_c^2(\mathbf{x}_c) = 0 \text{ on } \partial\Omega_{\square}^c, \quad (16)$$

$$\mathbf{v}_c(\mathbf{x}_c) = \mathbf{0} \text{ on } \partial\Omega_{\square}^c, \quad (17)$$

$$v_c^\alpha(\mathbf{x}_c) = \frac{d[R(\theta)]_{\alpha\beta}}{dt} [\psi^{t\beta}(\mathbf{x}_c) - f^\beta] \text{ on } \partial\Omega_{\square}^c, \quad (18)$$

$$\eta_F \frac{\partial v_c^\alpha}{\partial x_c^1} = 0 \text{ on } \partial\Omega_{\square}^c, \quad (19)$$

$$\sigma_c(\mathbf{x}_c) = 0 \text{ on } \partial\Omega_{\square}^c. \quad (20)$$

Equations (15) and (16) ensure that  $\mathbf{F}$  is injected on the boundary  $\partial\Omega_{\square}^c$  in a direction parallel to

the  $x_c^1$  axis, and Eq. (17) is a no-slip BC [5] along the channel walls  $\partial\Omega_{\square}^c$ , see Fig. 1. Equation (18) ensures that, at the boundary  $\partial\Omega_{\square}^c$ , the  $\mathbf{F}$  velocity matches the rotational velocity of  $\mathbf{R}$ . Given that  $\mathbf{R}$  can only rotate about its left focal point  $\mathbf{f}$ , the  $\mathbf{R}$  rotational velocity of a point  $\mathbf{x}_c \in \partial\Omega_{\square}^c$  is given by

$$\frac{d[R(\theta)]_{\alpha\beta}}{dt}[\psi^{t\beta}(\mathbf{x}_c) - c_\beta], \quad (21)$$

where  $\mathbf{R}$  is the rotation matrix corresponding to a counterclockwise rotation:

$$\mathbf{R}(\theta) \equiv \begin{pmatrix} \cos \theta & -\sin \theta \\ \sin \theta & \cos \theta \end{pmatrix}. \quad (22)$$

Finally, Eqs. (19) and (20) ensure, respectively, that on  $\partial\Omega_{\square}^c$  there is zero traction and tension; this corresponds to the hypothesis that there is free flow at  $\partial\Omega_{\square}^c$  [5, 8].

## 2. Equations of motion in the *reference*-configuration coordinates

For each field  $\mathbf{v}_c(\mathbf{x}_c), \sigma_c(\mathbf{x}_c)$  which depends on the coordinate  $\mathbf{x}_c$  in the  $\text{c}$  configuration, we introduce its counterpart in the  $\text{r}$  configuration:

$$\mathbf{v}_c(\mathbf{x}_r, t) \equiv \mathbf{v}_r(\varphi^t(\mathbf{x}_r), t), \quad (23)$$

$$\sigma_c(\mathbf{x}_r, t) \equiv \sigma_r(\varphi^t(\mathbf{x}_r), t). \quad (24)$$

We will now rewrite the equations of motion and the BCs in terms of  $\mathbf{v}_c, \sigma_c$ , and the  $\text{r}$  coordinate  $\mathbf{x}_r$ . The equations of motion (13) and (14) yield

$$\rho_F \left\{ \frac{\partial v_r^\alpha(\mathbf{x}_r, t)}{\partial t} + \left[ v_r^\gamma(\mathbf{x}_r, t) - \frac{d\varphi^t(\mathbf{x}_r)}{dt} \right] G_{\beta\gamma}(\mathbf{u}_D^t(\mathbf{x}_r)) \frac{\partial v_r^\alpha(\mathbf{x}_r, t)}{\partial x_r^\beta} \right\} = G_{\beta\alpha}(\mathbf{u}_D^t(\mathbf{x}_r)) \frac{\partial \sigma_r(\mathbf{x}_r, t)}{\partial x_r^\beta} + \eta_F G_{\delta\beta}(\mathbf{u}_D^t(\mathbf{x}_r)) \frac{\partial}{\partial x_r^\delta} \left[ G_{\gamma\beta}(\mathbf{u}_D^t(\mathbf{x}_r)) \frac{\partial v_r(\mathbf{x}_r, t)}{\partial x_r^\gamma} \right], \quad (25)$$

$$G_{\beta\alpha}(\mathbf{u}_D^t(\mathbf{x}_r)) \frac{\partial v_r^\alpha(\mathbf{x}_r, t)}{\partial x_r^\beta} = 0, \quad (26)$$

which hold in  $\Omega^r$ .

The BCs (15) to (20) are rewritten as

$$v_r^1(\mathbf{x}_r) = v_* \text{ on } \partial\Omega_{\square}^r, \quad (27)$$

$$v_r^2(\mathbf{x}_r) = 0 \text{ on } \partial\Omega_{\square}^r, \quad (28)$$

$$\mathbf{v}_r(\mathbf{x}_r) = \mathbf{0} \text{ on } \partial\Omega_{\square}^r, \quad (29)$$

$$v_r^\alpha(\mathbf{x}_r) = \frac{d[R(\theta)]_{\alpha\beta}}{dt}[x_r^\beta - f^\beta] \text{ on } \partial\Omega_{\square}^r, \quad (30)$$

$$\eta_F G_{\beta 1}(\mathbf{u}_D^t(\mathbf{x}_r)) \frac{\partial v_r^\alpha}{\partial x_r^\beta} = 0 \text{ on } \partial\Omega_{\square}^r, \quad (31)$$

$$\sigma_r(\mathbf{x}_r) = 0 \text{ on } \partial\Omega_{\square}^r. \quad (32)$$

## C. Motion of bulk fluid domain

The equations of motion (10) and (25) to (32) involve the displacement field  $\mathbf{u}_D$ , which describes

how the region—or domain—which contains  $\mathbf{F}$ , is deformed in time, cf. Fig. 1. We will denote this region as the  $\mathbf{D}$ . We observe that this field has, so far, been left arbitrary, and we have the freedom to choose it.

Here,  $\mathbf{u}_D$  will be determined with an analogy with the theory of elasticity [2]. We imagine that, as  $\mathbf{R}$  rotates about its focal point, each point  $\mathbf{x}_r \in \Omega^r$  moves into a point  $\mathbf{x}_c \in \Omega^c$ , and that the domain  $\Omega^r$  is deformed, e.g., locally stretched and compressed, into  $\Omega^c$ , like an elastic medium.

We will thus determine  $\mathbf{u}_D$  as the solution of a **boundary-value problem** (BVP) given by the following elastic model [2, 9]

$$\frac{\partial S_{D\alpha\beta}(\mathbf{u}_D)}{\partial x_r^\beta} = 0 \text{ in } \Omega^r, \quad (33)$$

where the elastic stress tensor  $S_D$  is given by

$$S_{D\alpha\beta} \equiv F_{\alpha\gamma} T_{\gamma\beta}, \quad (34)$$

(39) and (40), we obtain, respectively,

$$\frac{\partial}{\partial x_r^\beta} \frac{dS_{D\alpha\beta}(\mathbf{u}_D)}{dt} = 0 \text{ in } \Omega^r, \quad (41)$$

and

$$\begin{aligned} \dot{\mathbf{u}}_D &= \mathbf{0} \text{ on } \partial\Omega_\square^r, \\ \dot{\mathbf{u}}_D &= \omega \frac{d\mathbf{R}}{d\theta} \cdot (\mathbf{x}_r - \mathbf{f}) \text{ on } \partial\Omega_\circlearrowleft^r, \end{aligned} \quad (42) \quad (43)$$

$$T_{\alpha\beta} \equiv K(\mathbf{u}_D) E_{\gamma\gamma} \delta_{\alpha\beta} + 2\mu(\mathbf{u}_D) \left[ E_{\alpha\beta} - \frac{1}{2} \delta_{\alpha\beta} E_{\gamma\gamma} \right], \quad (35)$$

$$E_{\alpha\beta} \equiv \frac{1}{2} (F_{\gamma\alpha} F_{\gamma\beta} - \delta_{\alpha\beta}), \quad (36)$$

$$K(\mathbf{u}) \equiv \frac{1}{[\det(F(\mathbf{u}))]^\zeta}, \quad (37)$$

$$\mu(\mathbf{u}) \equiv \frac{1}{[\det(F(\mathbf{u}))]^\zeta}. \quad (38)$$

In Eqs. (37) and (38), we included an additional dependence of bulk modulus  $K$  and the modulus of compression  $\mu$  on the deformation-gradient tensor (2). In the absence of this dependence, the elastic model above would be unstable under local compression. In fact, the model's Lagrangian would not penalize configurations with small  $\det F$ . The inclusion of the dependence (37) and (38) on  $\det F$  allows for penalizing these configurations—the larger the exponent  $\zeta > 0$ , the stronger the penalty. As a result, this dependence makes the model stable under mesh compression, such as the one shown below  $\mathbf{R}$  in Fig. 1B.

The BCs for the partial differential equation (PDE) (33) are

$$\mathbf{u}_D = \mathbf{0} \text{ on } \partial\Omega_\square^r, \quad (39)$$

$$\mathbf{u}_D = \mathbf{f} - \mathbf{x}_r + \mathbf{R}(\theta) \cdot (\mathbf{x}_r - \mathbf{f}) \text{ on } \partial\Omega_\circlearrowleft^r. \quad (40)$$

Equation (39) enforces the fact that the mesh is not deformed at the boundary  $\partial\Omega_\square^r$ . Finally, Eq. (40) ensures that the mesh deformation at  $\partial\Omega_\circlearrowleft^r$  matches the deformation induced by the rotation of  $\mathbf{R}$ .

Equations (33), (39) and (40) constitute the BVP which determines  $\mathbf{u}_D$ . Along the lines of BVPs in the theory of elasticity, such BVP is already, naturally formulated in the  $\mathbf{r}$  configuration [3].

From the BVP above, we obtain a BVP for  $\dot{\mathbf{u}}_D$ , which will be needed in the following to describe the  $\mathbf{D}$  motion. By deriving both sides of Eqs. (33),

where in Eqs. (42) and (43) we used the fact that  $\mathbf{x}_r$  is independent of time, and in Eq. (43) we substituted Eq. (8). The left-hand side (LHS) of Eq. (41) depends on the second partial derivatives of  $\mathbf{u}_D$  and  $\dot{\mathbf{u}}_D$ —see Eqs. (34) to (38). As a result, given  $\theta$ ,  $\omega$ , and  $\mathbf{u}_D$  from Eqs. (33), (39) and (40), the BVP (41) to (43) yields  $\dot{\mathbf{u}}_D$ .

Overall Eqs. (8), (10), (25) to (33) and (39) to (43) constitute a BVP for  $\theta, \omega, \mathbf{v}_r, \sigma_r, \mathbf{u}_D$  and  $\dot{\mathbf{u}}_D$  which, combined with the temporal BCs

$$\theta(t=0) = \theta_0 \quad (44)$$

$$\omega(t=0) = \omega_0 \quad (45)$$

$$\mathbf{v}_r(\mathbf{x}_r, t=0) = \mathbf{v}_{r0}(\mathbf{x}_r), \quad (46)$$

$$\sigma_r(\mathbf{x}_r, t=0) = \sigma_{r0}(\mathbf{x}_r), \quad (47)$$

determine the dynamics of the system.

## D. Temporal discretization

To numerically solve for the dynamics in a time span  $0 \leq t \leq T$ , we discretize time by setting  $\Delta t \equiv T/N$ ,  $t_n \equiv n \Delta t$ , with  $n = 0, 1, \dots, N$ .

We combine the Crank Nicolson (CN) discretization method for NS equations [8, 10] with the ALE formulation, by discretizing the dynamical equations for  $\mathbf{R}$ ,  $\mathbf{F}$  and  $\mathbf{D}$ —see below.

### 1. Rigid body

Proceeding along the CN scheme [10], we define fields at staggered, integer and semi-integer time steps scheme [8]. We set

$$\sigma_r^n(\mathbf{x}_r) \equiv \sigma_c(\mathbf{x}_r, t_n) \quad (48)$$

$$\sigma_r^{n-1/2}(\mathbf{x}_r) \equiv \sigma_c \left( \mathbf{x}_r, \frac{t_n + t_{n-1}}{2} \right), \quad (49)$$

and similarly for other quantities.

We discretize Eqs. (8) and (10) and, neglecting  $\mathcal{O}(\Delta t)$ , we obtain

$$\frac{\theta^n - \theta^{n-1}}{\Delta t} = \omega^n, \quad (50)$$

$$\begin{aligned} \frac{\omega^n - \omega^{n-1}}{\Delta t} &= I \int_{\partial\Omega_r^c} ds \epsilon_{\alpha\beta} [\xi^\alpha(s) + u^{n-1,\alpha}(\xi(s)) - f^\alpha] \varsigma_{\beta\gamma}^{r,n-1}(\xi(s); \mathbf{v}_r^{n-1}, \sigma_r^{n-3/2}) \times \\ &\quad \epsilon_{\gamma\lambda} F_{\lambda\mu}(\mathbf{u}_D^{n-1}(\xi(s))) \frac{d\xi^\mu(s)}{ds}, \end{aligned} \quad (51)$$

where in Eq. (51) we used Eqs. (1) and (5) and we explicitly indicated the dependence of the stress tensor (11) on  $\mathbf{v}_c$  and  $\sigma_c$ .

## 2. Bulk fluid

To discretize in time the **F** problem, we will apply the **CN** splitting scheme [8, 10] to the **NS** equations

---

(25) and (26) in the **r** configurations. This splitting scheme is derived from the **incremental pressure correction scheme** [11], in which the solution of the **NS** equations is split into three intermediate steps. In what follows, we will synonymously use the terms ‘pressure’ and ‘surface tension’ for conciseness [12].

The discrete form of the PDEs Eqs. (25) and (26) is

$$\rho_F \left[ \frac{v_r^{n,\alpha} - v_r^{n-1,\alpha}}{\Delta t} + \frac{3}{2}(v_r^{n-1,\gamma} - \dot{u}^{n-1,\gamma}) G_{\beta\gamma}(\mathbf{u}_D^{n-1}) \frac{\partial v_r^{n-1,\alpha}}{\partial x_r^\beta} - \frac{1}{2}(v_r^{n-2,\gamma} - \dot{u}^{n-2,\gamma}) \times \right. \quad (52)$$

$$\begin{aligned} &\left. G_{\beta\gamma}(\mathbf{u}_D^{n-2}) \frac{\partial v_r^{n-2,\alpha}}{\partial x_r^\beta} \right] = \\ &G_{\beta\alpha}(\mathbf{u}_D^{n-1}) \frac{\partial \sigma_r^{n-1/2}}{\partial x_r^\beta} + \eta_F G_{\delta\beta}(\mathbf{u}_D^{n-1}) \frac{\partial}{\partial x_r^\delta} \left[ G_{\gamma\beta}(\mathbf{u}_D^{n-1}) \frac{\partial}{\partial x_r^\gamma} \left( \frac{v_r^{n,\alpha} + v_r^{n-1,\alpha}}{2} \right) \right], \\ &G_{\beta\alpha}(\mathbf{u}_D^{n-1}) \frac{\partial v_r^{n,\alpha}}{\partial x_r^\beta} = 0, \end{aligned} \quad (53)$$

where we omitted the dependence on  $\mathbf{x}_r$  for clarity. Also, in the **LHS** of Eq. (52) we rewrote the convective term according to the Adams-Bashforth discretization scheme [8, 13], and we used Eqs. (1)

---

and (5) to rewrite the time derivative of  $\varphi$  in terms of  $\dot{\mathbf{u}}_D$ .

The discrete form of the **BCs** (27) to (32) reads

$$v_r^{n,1} = v_* \text{ on } \partial\Omega_{\square}^r, \quad (54)$$

$$v_r^{n,2} = 0 \text{ on } \partial\Omega_{\square}^r, \quad (55)$$

$$\mathbf{v}_r^n = \mathbf{0} \text{ on } \partial\Omega_{\square}^r, \quad (56)$$

$$\mathbf{v}_r = \omega^n \left. \frac{d\mathbf{R}}{d\theta} \right|_{\theta=\theta_n} \cdot (\mathbf{x}_r - \mathbf{f}) \text{ on } \partial\Omega_{\square}^r, \quad (57)$$

$$\eta_F G_{\beta 1}(\mathbf{u}_D^{n-1}) \frac{\partial}{\partial x_r^\beta} \left( \frac{v_r^{n,\alpha} + v_r^{n-1,\alpha}}{2} \right) = 0 \text{ on } \partial\Omega_{\square}^r, \quad (58)$$

$$\sigma_r^{n-1/2} = 0 \text{ on } \partial\Omega_{\square}^r. \quad (59)$$

We will now split the **BVP** into three steps [8, 14]:

the velocity  $\bar{\mathbf{v}}$ , which approximates the true velocity  $\mathbf{v}_r$ , and which satisfies the **BVP**

**1. Approximated velocity.** We introduce

$$\rho_F \left\{ \frac{\bar{v}^\alpha - v_r^{n-1,\alpha}}{\Delta t} + \left[ \frac{3}{2}(v_r^{n-1,\gamma} - \dot{u}^{n-1,\gamma}) G_{\beta\gamma}(\mathbf{u}_D^{n-1}) - \frac{1}{2}(v_r^{n-2,\gamma} - \dot{u}^{n-2,\gamma}) G_{\beta\gamma}(\mathbf{u}_D^{n-2}) \right] \frac{\partial V^\alpha}{\partial x_r^\beta} \right\} = (60)$$

$$G_{\beta\alpha}(\mathbf{u}_D^{n-1}) \frac{\partial \sigma_r^*}{\partial x_r^\beta} + \eta_F G_{\delta\beta}(\mathbf{u}_D^{n-1}) \frac{\partial}{\partial x_r^\delta} \left( G_{\gamma\beta}(\mathbf{u}_D^{n-1}) \frac{\partial V^\alpha}{\partial x_r^\gamma} \right),$$

$$\bar{v}^1 = v_* \text{ on } \partial\Omega_{\square}^r, \quad (61)$$

$$\bar{v}^2 = 0 \text{ on } \partial\Omega_{\square}^r, \quad (62)$$

$$\bar{\mathbf{v}} = \mathbf{0} \text{ on } \partial\Omega_{\square}^r, \quad (63)$$

$$\bar{\mathbf{v}} = \omega^n \left. \frac{d\mathbf{R}}{d\theta} \right|_{\theta=\theta_n} \cdot (\mathbf{x}_r - \mathbf{f}) \text{ on } \partial\Omega_{\square}^r, \quad (64)$$

$$\eta_F G_{\beta 1}(\mathbf{u}_D^{n-1}) \frac{\partial V^\alpha}{\partial x_r^\beta} = 0 \text{ on } \partial\Omega_{\square}^r. \quad (65)$$

where

$$\mathbf{V} \equiv \frac{\bar{\mathbf{v}} + \mathbf{v}_r^{n-1}}{2}, \quad (66)$$

$$\sigma_r^* \equiv \sigma_r^{n-3/2}. \quad (67)$$

**2. Pressure correction.**

Subtracting Eqs. (52) and (60) and neglecting  $\mathcal{O}(\Delta t)$ , we obtain

$$\rho_F \frac{\bar{v}^\alpha - v_r^{n,\alpha}}{\Delta t} = G_{\beta\alpha}(\mathbf{u}_D^{n-1}) \frac{\partial \phi}{\partial x_r^\beta} \text{ in } \Omega^r, \quad (68)$$

where

$$\phi \equiv \sigma_c^* - \sigma_c^{n-1/2} \quad (69)$$

is the surface-tension increment. By applying  $G_{\gamma\alpha}(\mathbf{u}_D^{n-1}) \partial/\partial x_r^\gamma$  to both sides of Eq. (68) and using Eq. (53), we obtain a second-order PDE for  $\phi$ :

$$\frac{\rho_F}{\Delta t} G_{\gamma\alpha}(\mathbf{u}_D^{n-1}) \frac{\partial \bar{v}^\alpha}{\partial x_r^\gamma} = (70)$$

$$G_{\gamma\alpha}(\mathbf{u}_D^{n-1}) \frac{\partial}{\partial x_r^\gamma} \left( G_{\beta\alpha}(\mathbf{u}_D^{n-1}) \frac{\partial \phi}{\partial x_r^\beta} \right).$$

We will now work out the BCs for Eq. (70). Equations (59), (67) and (69) imply the BC

$$\phi = 0 \text{ on } \partial\Omega_{\square}^r. \quad (71)$$

Multiplying Eq. (68) by  $G_{\gamma\alpha}(\mathbf{u}_D^{n-1})\hat{\mathbf{n}}^r\gamma$ , where  $\hat{\mathbf{n}}^r$  is the unit boundary normal in the  $r$  configuration, we obtain

$$\frac{\rho_F}{\Delta t} G_{\gamma\alpha}(\mathbf{u}_D^{n-1})\hat{\mathbf{n}}^r\gamma(\bar{v}^\alpha - v_r^{n,\alpha}) = \quad (72)$$

$$\hat{\mathbf{n}}^r\gamma G_{\gamma\alpha}(\mathbf{u}_D^{n-1})G_{\beta\alpha}(\mathbf{u}_D^{n-1})\frac{\partial\phi}{\partial x_r^\beta}.$$

Combining Eq. (72) with Eqs. (54) to (57) and (61) to (64), we obtain the second BC

$$\hat{\mathbf{n}}^r\gamma G_{\gamma\alpha}(\mathbf{u}_D^{n-1})G_{\beta\alpha}(\mathbf{u}_D^{n-1})\frac{\partial\phi}{\partial x_r^\beta} = \quad (73)$$

$$0 \text{ on } \partial\Omega_D^r \cup \partial\Omega_\square^r \cup \partial\Omega_\bullet^r.$$

The BVP (70), (71) and (73) determines  $\phi$  and, through the definition (69), the surface tension  $\sigma_c^{n-1/2}$ .

- 3. Velocity correction.** The velocity  $\mathbf{v}_r^n$  is determined from the approximate velocity  $\bar{\mathbf{v}}$  from Eq. (68).

### 3. Bulk fluid domain

The discrete version of the BVP for  $\mathbf{u}_D$ , Eqs. (33), (39) and (40), reads

$$\frac{\partial S_{D\alpha\beta}(\mathbf{u}_D^n)}{\partial x_r^\beta} = 0 \text{ in } \Omega^r, \quad (74)$$

$$\mathbf{u}_D^n = \mathbf{0} \text{ on } \partial\Omega_\square^r, \quad (75)$$

$$\mathbf{u}_D^n = \mathbf{f} - \mathbf{x}_r + \mathbf{R}(\theta^n) \cdot (\mathbf{x}_r - \mathbf{f}) \text{ on } \partial\Omega_\bullet^r, \quad (76)$$

and that of the BVP for  $\dot{\mathbf{u}}_D$ , Eqs. (41) to (43), is

$$\frac{\partial}{\partial x_r^\beta} \frac{dS_{D\alpha\beta}(\dot{\mathbf{u}}_D^n)}{dt} = 0 \text{ in } \Omega^r, \quad (77)$$

$$\dot{\mathbf{u}}_D^n = \mathbf{0} \text{ on } \partial\Omega_\square^r, \quad (78)$$

$$\dot{\mathbf{u}}_D^n = \omega \frac{d\mathbf{R}}{d\theta} \cdot (\mathbf{x}_r - \mathbf{f}) \text{ on } \partial\Omega_\bullet^r, \quad (79)$$

We can now iterate in time for the ensemble of fields as follows. At each step  $n$ , given  $\theta^{n-1}$ ,  $\omega^{n-1}$ ,  $\mathbf{v}_r^{n-1}$ ,  $\sigma_r^{n-3/2}$ ,  $\mathbf{u}_D^{n-1}$  and  $\dot{\mathbf{u}}_D^{n-1}$  from the preceding step, we

- 1. Update R.** Solve the algebraic equations Eqs. (50) and (51) for  $\theta^n$  and  $\omega^n$ .

- 2. Update D.** Solve the BVPs (74) to (79) for  $\mathbf{u}_D^n$  and  $\dot{\mathbf{u}}_D^n$ .

- 3. Update F.** Solve the BVPs (60) to (65) and (71) to (73) for  $\bar{\mathbf{v}}$  and  $\sigma_r^{n-1/2}$ , and obtain  $\mathbf{v}_r^n$  from Eq. (68).

The fields  $\mathbf{v}_r^{n-1}$ ,  $\sigma_r^{n-3/2}$  in the  $c$  configuration are then obtained from the respective fields in the  $r$  configuration through Eqs. (23) and (24).

An example of such dynamics is shown in Fig. 2. The channel has dimensions  $L = 2.2$  m,  $h = 0.41$  m, cf. Fig. 1,  $\rho_F = 1$  Kg/m<sup>2</sup>,  $\eta_F = 10^{-3}$  Pa m sec, and the inflow velocity profile is a Poiseuille flow  $v_*(\mathbf{x}_c) = 6v_0x_c^2(x_c^2 - h)/h^2$ , with  $v_0 = 1$  m/sec. These parameters have been taken from the FEAT2D DFG 2D-3 benchmark for a flow around a cylinder [15]. The  $D$  mesh stiffness exponent has been chosen to be  $\zeta = 3$  [2]. Finally,  $R$  is an ellipse with semi-axes  $a = 0.1$  m,  $b = 0.075$  m, center located at  $\mathbf{x}_r = (0.25$  m,  $0.2$  m), and moment of inertia  $I = 10^{-1}$  Kg m<sup>2</sup>. These parameters correspond approximately to a light gas interacting with a solid body made of light wood.

As shown in Fig. 3, the dynamics of Fig. 2 involves two physical time scales: A short one,  $\tau_S$ , related to fast angular oscillations of  $B$ , and a long one,  $\tau_L$ , given by the damping of such oscillations.

First, the scale  $\tau_S$  can be estimated by considering the dynamical equation (7) for  $B$ , and approximating its LHS as  $I/\tau_S^2$  and its RHS as  $(\eta_F v_0/a)2\pi a$ . Here,  $\eta_F v_0/a$  is the viscous component of the force per unit length exerted by  $F$  on  $B$ , cf. Eq. (9),  $2\pi a$  estimates the total length of the boundary of  $B$ , and  $a$  approximates the lever arm of the force above. Putting everything together, we obtain

$$\tau_S \sim \sqrt{\frac{I}{2\pi a \eta_F v_0}}. \quad (80)$$

For the parameters of Fig. 2, Eq. (80) yields  $\tau_S \sim 13$  sec, which is in agreement with the period of the oscillations in Fig. 3.

Second,  $\tau_L$  can be estimated by building a combination of the material parameters  $\rho_F$ ,  $\eta_F$  and  $I$  of the model. The only parameter combination that can yield a quantity with the dimensions of a time is

$$\tau_L \sim \frac{\sqrt{\rho_F I}}{\eta_F}. \quad (81)$$

For the parameters of Fig. 2, Eq. (81) yields  $\tau_L \sim 316$  sec, which is roughly the timescale at which

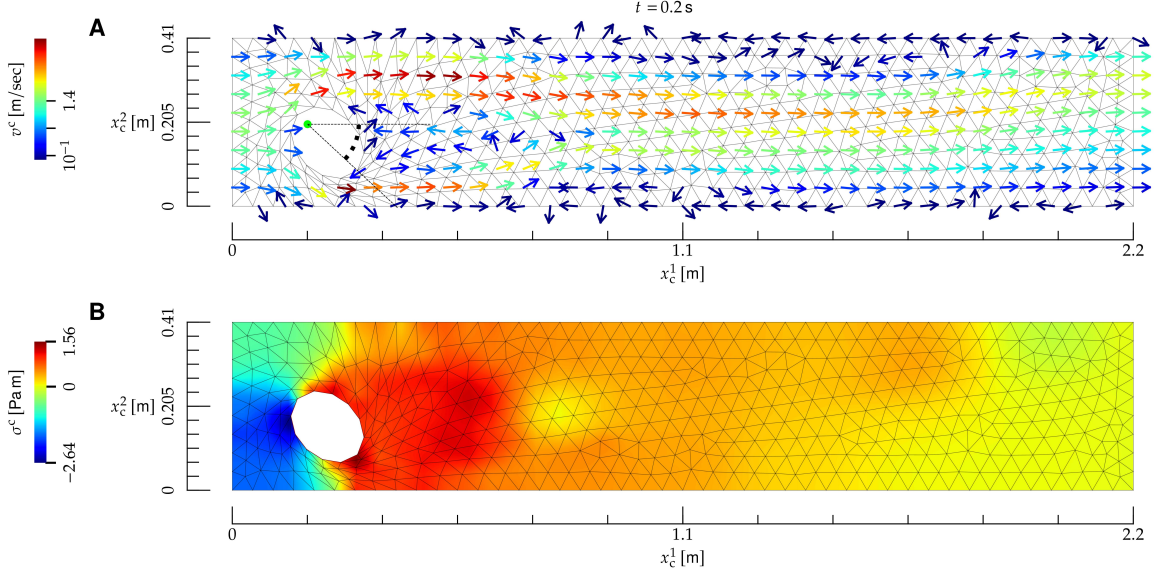


**FIG. 2:** Interaction between a **bulk fluid** and a rigid **body**, whose material properties roughly correspond to a light gas and a body made of light wood, respectively. **A)** Temporal snapshot of the mesh (black lines) and velocity field (arrows) at the **current** time  $t$ , shown on top. The direction of the velocity field is indicated by the arrows, and its norm by their color; the direction of arrows with velocity close to zero is not defined. The **body** (ellipse) is allowed to pivot about its left focal point (red dot), and the related angle with respect to the  $x_c^1$  direction is denoted by a red arc. **B)** Color map of the surface tension at the **current** instant of time  $t$ .

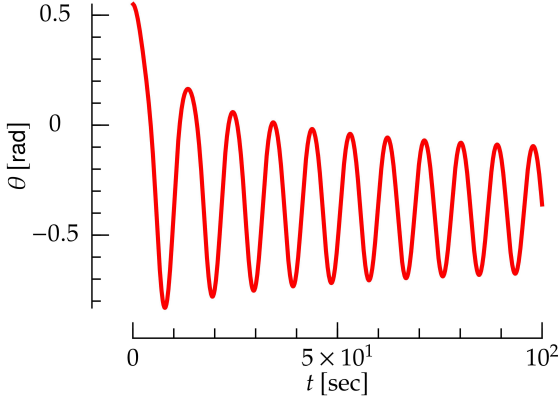


**FIG. 3:** Angle of the **body** as a function of time for the interaction between a **bulk fluid** and a rigid **body** shown in Fig. 2.

## II. FLUID AND ELASTIC BODY

In this Section, we will build on the analysis of Section I and put F into interaction with a more complex physical object: an **elastic body** (E). Only the main results will be presented here; their derivation follows the lines of Section I.

The **r** and **c** configurations are shown in Fig. 4. Here, the **E** boundary  $\partial\Omega_O$  may deform, but the inner **E** boundary  $\partial\Omega_\bullet$  is pinned to the  $x^1$ ,  $x^2$  plane.

The equations of motion are the following.

First, the dynamics of F is governed by the **NS** and mass-conservation equations (13) and (14), respectively. Their **BCs** are Eqs. (15) to (17), (19) and (20), which stay unchanged. On the other hand, **BC** (18), which ensures that the F velocity matches the B velocity at the interface between F and B, now reads

$$\mathbf{v}_c(\mathbf{x}_c) = \frac{d\mathbf{u}_E(\mathbf{x}_r)}{dt} \Big|_{\mathbf{x}_r=\psi^t(\mathbf{x}_c)} \quad \text{on } \partial\Omega_O^c \quad (82)$$

the width of the oscillations in Fig. 3 is dampened out.

Second, the motion of E is governed by Newton's

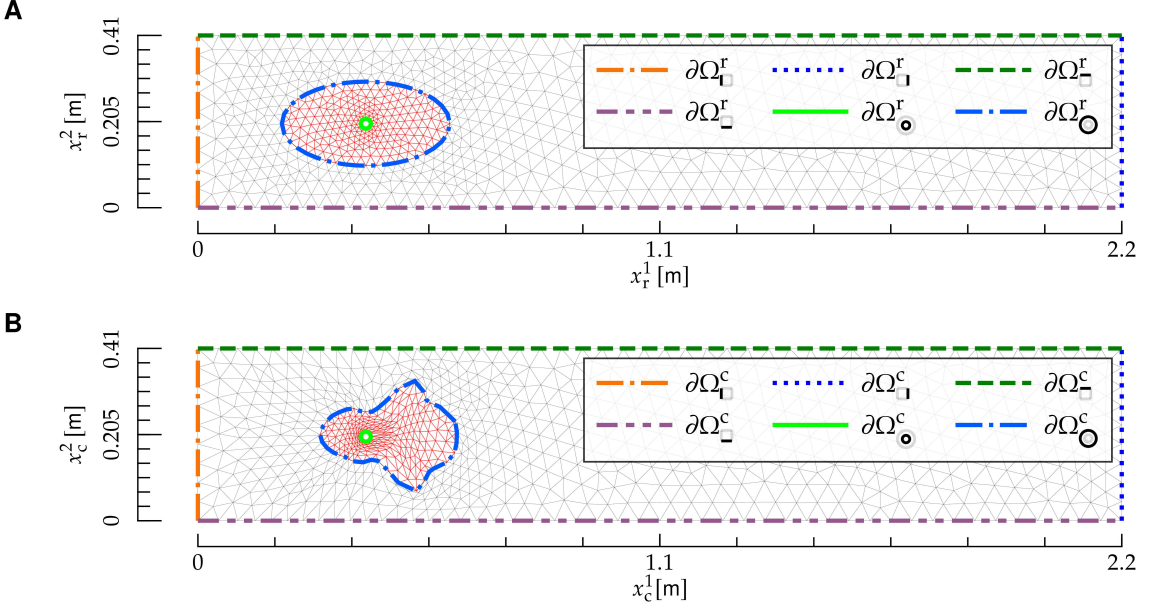


**FIG. 4:** Reference and current configuration for the interaction between a bulk fluid and an elastic body. The figures follows the same notation as Fig. 1.

equations of motion for an elastic body [3]

$$\rho_E \frac{d^2 u_E^\alpha(x_r)}{dt^2} = \frac{\partial S_{E\alpha\beta}(u_E)}{\partial x_r^\beta}, \quad (83)$$

where  $u_E$  and  $\rho_E$  are, respectively, the deformation field and density of E; the latter is assumed to be independent of space. The E stress tensor is derived from a compressible neo-Hookean model [16], and it reads

$$S_{E\alpha\beta} \equiv \frac{\mu}{\det(F)} \left( -\frac{1}{2} C_{\gamma\gamma} G_{\alpha\beta} + F_{\beta\alpha} \right) + K[(\det(F))^2 - 1] G_{\alpha\beta}, \quad (84)$$

where

$$C_{\alpha\beta} \equiv \delta_{\alpha\beta} + 2E_{\alpha\beta}. \quad (85)$$

We have chosen this model because it is stable under compression, i.e., its potential energy diverges as  $\det(F) \rightarrow 0$  [16]. As opposed to linear models [3] and to the elastic model of Section I C, this model proves to yield a stable dynamics for E as it is compressed by F, see below and Fig. 5. The BCs

for Eq. (83) are

$$u_E(x_r) = 0 \text{ on } \partial\Omega_r^r, \quad (86)$$

$$\epsilon_{\beta\gamma} S_{E\alpha\beta}(u_E^t)|_{x_r=\xi(s)} \frac{d\xi^\gamma}{ds} = \zeta^c{}_{\alpha\beta}(\varphi^t(\xi(s))) \epsilon_{\beta\gamma} \frac{d\varphi^{t,\gamma}(\xi(s))}{ds} \text{ on } \partial\Omega_O^r. \quad (87)$$

Finally, the equations of motion for D are (33) and (41), with BCs (39) and (42) and

$$u_D^t(x_r) = u_E^t(x_r) \text{ on } \partial\Omega_O^r, \quad (88)$$

$$\dot{u}_D^t(x_r) = \dot{u}_E^t(x_r) \text{ on } \partial\Omega_O^r. \quad (89)$$

Equation (88) and Eq. (89) ensure that the displacement and velocity of E and D are conformal at the E-D interface, and they replace Eqs. (40) and (43), respectively.

The system dynamics is obtained as follows: given  $v_r^{n-1}$ ,  $\sigma_r^{n-3/2}$ ,  $u_E^{n-1}$ ,  $\dot{u}_E^{n-1}$ ,  $u_D^{n-1}$  and  $\dot{u}_D^{n-1}$  from the preceding step, we

- **Update E.** Solve for  $u_E^n$  and  $\dot{u}_E^n$  the discrete version of Eq. (83)

$$\rho_E \frac{\dot{u}_E^{n,\alpha} - \dot{u}_E^{n-1,\alpha}}{\Delta t} = \frac{\partial S_{E\alpha\beta}(u_E^n)}{\partial x_r^\beta}, \quad (90)$$

$$\frac{u_E^n - u_E^{n-1}}{\Delta t} = \dot{u}_E, \quad (91)$$

with BCs obtained from Eqs. (86) and (87):

$$\mathbf{u}_E^n = 0 \text{ on } \partial\Omega_{\bullet}^r, \quad (92)$$

$$\epsilon_{\beta\gamma} S_{E\alpha\beta}(\mathbf{u}_E^n) \Big|_{x_r=\xi(s)} \frac{d\xi^\gamma}{ds} = \varsigma^r_{\alpha\beta}(\xi(s); \mathbf{v}_r^{n-1}, \sigma_r^{n-3/2}, \mathbf{u}^n) \epsilon_{\beta\gamma} F_{\gamma\delta}(\mathbf{u}_E^{n-1}) \Big|_{x_r=\xi(s)} \frac{d\xi^\delta}{ds} \text{ on } \partial\Omega_{\bullet}^r. \quad (93)$$

In Eq. (93), we have used Eqs. (2) and (5) to rewrite the derivative of  $\phi(\xi(s))$ .

- **Update D.** Solve for  $\mathbf{u}_D^n$  and  $\dot{\mathbf{u}}_D^n$  the **BVPs** given by Eqs. (74) and (77) with **BCs** (75), (78) and

$$\mathbf{u}_D^n = \mathbf{u}_E^n \text{ on } \partial\Omega_{\bullet}^r, \quad (94)$$

$$\dot{\mathbf{u}}_D^n = \dot{\mathbf{u}}_E^n \text{ on } \partial\Omega_{\bullet}^r. \quad (95)$$

- **Update F.** Solve the **BVPs** given by (60) and (70) and **BCs** (61) to (63), (65), (71) and (73) and

$$\mathbf{v}_r = \dot{\mathbf{u}}_E \text{ on } \partial\Omega_{\bullet}^r, \quad (96)$$

which replaces Eq. (65) for a rigid body, and solve Eq. (68).

An example of the coupled dynamics of **F** and **E** is shown in Fig. 5. Here,  $\partial\Omega_{\bullet}^r$  is an ellipse

with semi-axes  $a = 0.2 \text{ m}$ ,  $b = 0.1 \text{ m}$  and center located at  $x_r = (0.4 \text{ m}, 0.2 \text{ m})$ , and  $\partial\Omega_{\bullet}^r$  has radius  $r = 0.0125 \text{ m}$  and center located at  $x_r$ . The **E** density and elastic moduli are, respectively,  $\rho_E = 10^3 \text{ Kg/m}^2$  and  $K = \mu = 10 \text{ Kg/sec}^2$ . The other parameters are the same as in Fig. 2.

### III. FLUID AND HELFRICH MEMBRANE

In this Section, we will build on the analysis of Section II, and complexify the structure of the elastic body with which **F** interacts by considering, instead of an elastic material, an **Helfrich membrane** (**M**) [1, 17]. Both the physical structure and mathematical description of **M** is significantly more complex than that of **E**. First, unlike **E**, **M** has a fluid structure: its material elements can flow both tangentially and normally to it. Such fluid behavior requires an Eulerian description, which then needs to be connected to the Lagrangian description used to describe **D**. Second, **M** is described by fourth-order PDEs [1], which is significantly more complex than the second-order PDEs which describe **E** [12].

The dynamical equations for **M** are

$$\nabla_i v^i - 2Hw = 0, \quad (97)$$

$$\rho(\partial_t v^i + v^j \nabla_j v^i - 2v^j w b_j^i - w \nabla^i w) =$$

$$\nabla^i \sigma + \eta [-\nabla_{LB} v^i - 2(b^{ij} - 2Hg^{ij}) \nabla_j w + 2Kv^i], \quad (98)$$

$$\rho [\partial_t w + v^i (v^j b_{ji} + \nabla_i w)] =$$

$$2\kappa [\nabla_{LB} H - 2H(H^2 - K)] + 2\sigma H + 2\eta [(\nabla^i v^j) b_{ij} - 2w(2H^2 - K)], \quad (99)$$

### ACKNOWLEDGMENTS

We would like to thank S. Al-Izzi and S. Astruc for useful discussions, and the **finite element computational software** (**FEnICS**) online community for

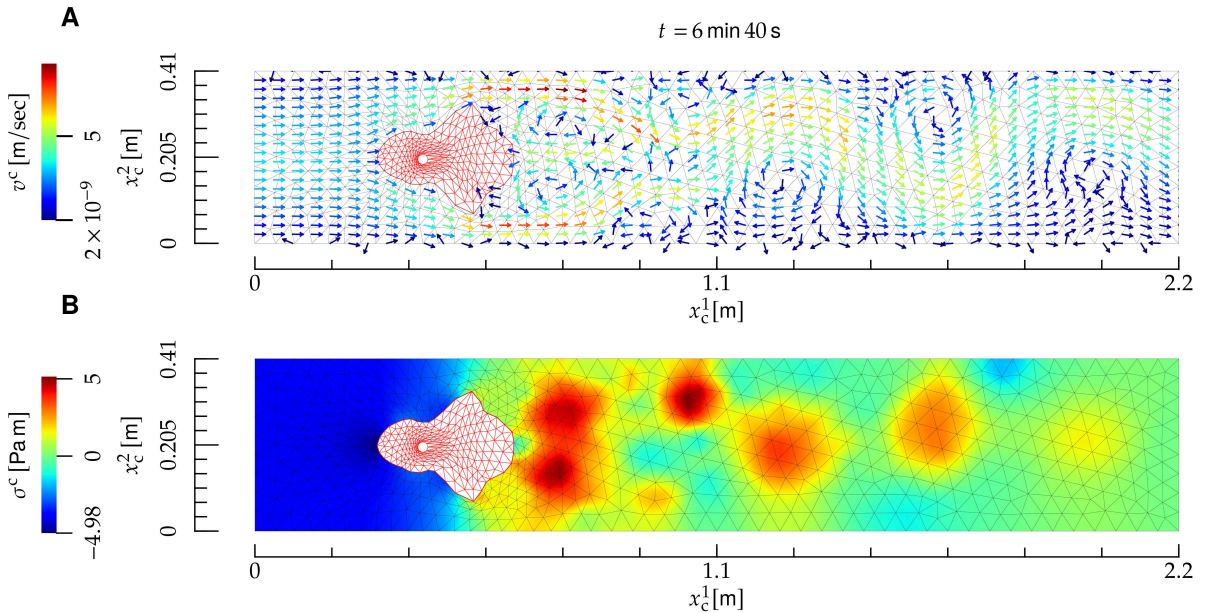


**FIG. 5:** Interaction between a **bulk fluid** and an **elastic body**. The notation is the same as in Fig. 2, and the **elastic body** is depicted as a red mesh.

its precious support.

This work was granted access to the high-

performance computing resources of MesoPSL financed by the Region Île de France, and to the Abacus cluster at Institut Curie.

- [1] I. Derényi, F. Jülicher, and J. Prost. Formation and Interaction of Membrane Tubes. *Phys. Rev. Lett.*, 88(23):238101, May 2002.
- [2] D. Kamensky. Lecture notes for MAE 207: Finite element analysis for coupled problems, 2022.
- [3] L. D. Landau and E. M. Lifshitz. *Theory of Elasticity*. Elsevier, 1986.
- [4] W. S. Slaughter. *The Linearized Theory of Elasticity*. Birkhäuser Boston, Boston, MA, 2002.
- [5] L. D. Landau and E. M. Lifschitz. *Fluid Mechanics*. Pergamon, 1987.
- [6] H. Goldstein, C. P. Poole, and J. L. Safko. *Classical Mechanics*. Pearson, 2004.
- [7] S. Marchiafava. *Appunti Di Geometria Differenziale*, volume I, II, III. Edizioni Nuova Cultura, 2005.
- [8] A. Logg, K.-A. Mardal, and G. Wells, editors. *Automated Solution of Differential Equations by the Finite Element Method: The FEniCS Book*, volume 84 of *Lecture Notes in Computational Science and Engineering*. Springer Berlin Heidelberg, Berlin, Heidelberg, 2012.
- [9] J. E. Marsden and T. J. R. Hughes. *Mathematical Foundations of Elasticity*. Dover, New York, 1994.
- [10] J. Crank and P. Nicolson. A practical method for

- numerical evaluation of solutions of partial differential equations of the heat-conduction type. *Math. Proc. Camb. Phil. Soc.*, 43(1):50–67, Jan. 1947.
- [11] K. Goda. A multistep technique with implicit difference schemes for calculating two- or three-dimensional cavity flows. *Journal of Computational Physics*, 30(1):76–95, Jan. 1979.
- [12] D. Wörthmüller, G. Ferraro, P. Sens, and M. Castellana. IRENE: A fluId layeR finite-elemeNt softwarE. <http://arxiv.org/abs/2506.17827>, July 2025.
- [13] *Solving Ordinary Differential Equations I*, volume 8 of *Springer Series in Computational Mathematics*. Springer Berlin Heidelberg, Berlin, Heidelberg, 1993.
- [14] A. J. Chorin. Numerical solution of the Navier-Stokes equations. *Math. Comp.*, 22(104):745–762, 1968.
- [15] H. Blum, J. Harig, S. Müller, S. Schreiber, and S. Turek. FEAT2D, Finite Element Analysis Tools User Manual, 1995.
- [16] Y. Bazilevs, V. M. Calo, T. J. R. Hughes, and Y. Zhang. Isogeometric fluid-structure interaction: Theory, algorithms, and computations. *Comput Mech*, 43(1):3–37, Dec. 2008.

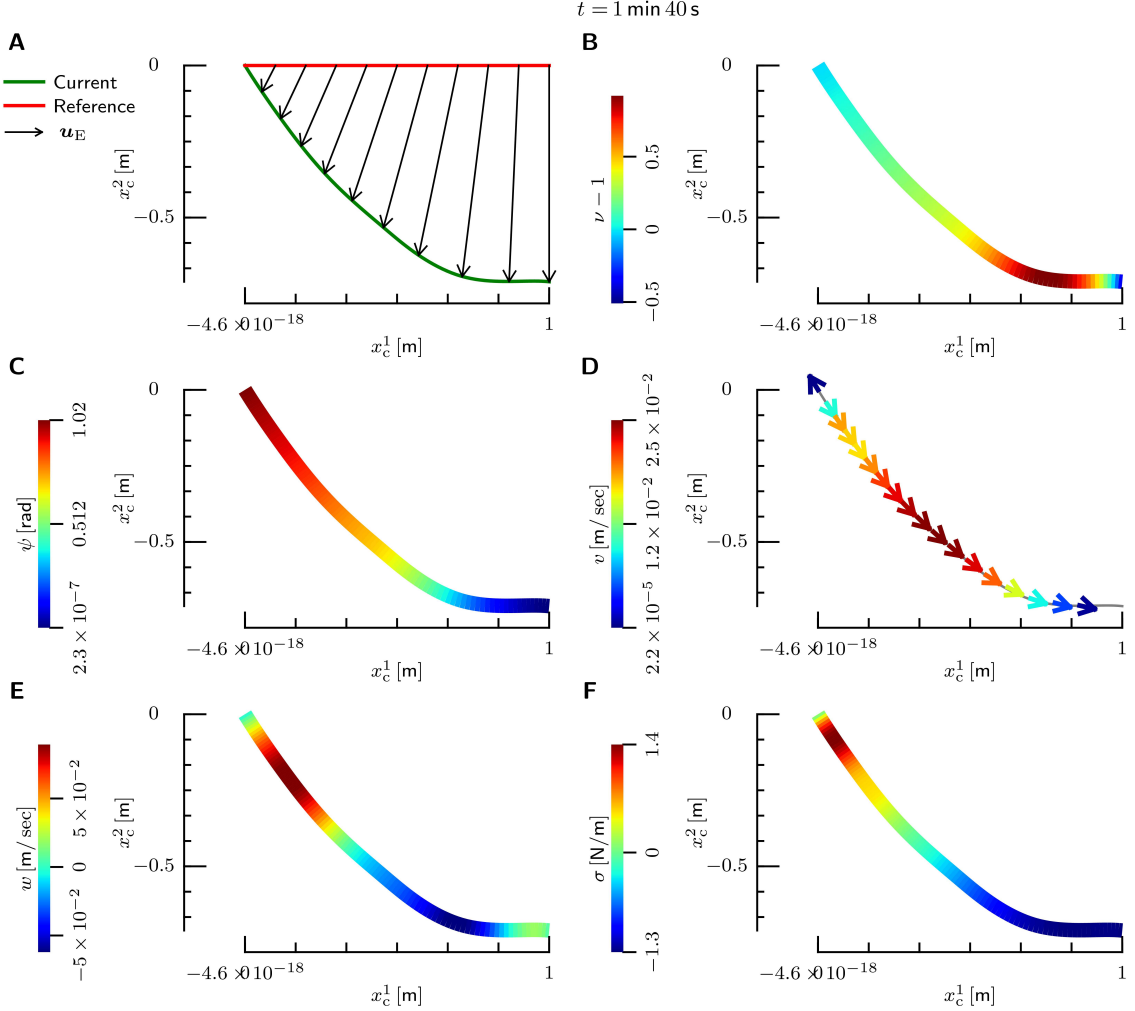


**FIG. 6:** Helfrich fluid layer described with the generalized arc length gauge. The layer is subjected to a gravitational field directed along the  $X^2$  axis, in the direction of negative  $X^2$ . **A)** Displacement field  $\vec{U}$ , which relates the reference and the current configuration, shown in red and green, respectively. **B)** Stretching  $\nu$ . **C)** Tangent angle  $\psi$ . **D)** Tangential velocity. Arrows show the velocity direction, and the color code the velocity norm. **E)** Normal velocity, whose value is shown with the color code. **F)** Surface tension. All panels refer to the same instant of time, shown on top.

[17] W. Helfrich. Elastic Properties of Lipid Bilayers: Theory and Possible Experiments. *Zeitschrift für Naturforschung C*, 28(11-12):693–703, Dec. 1973.

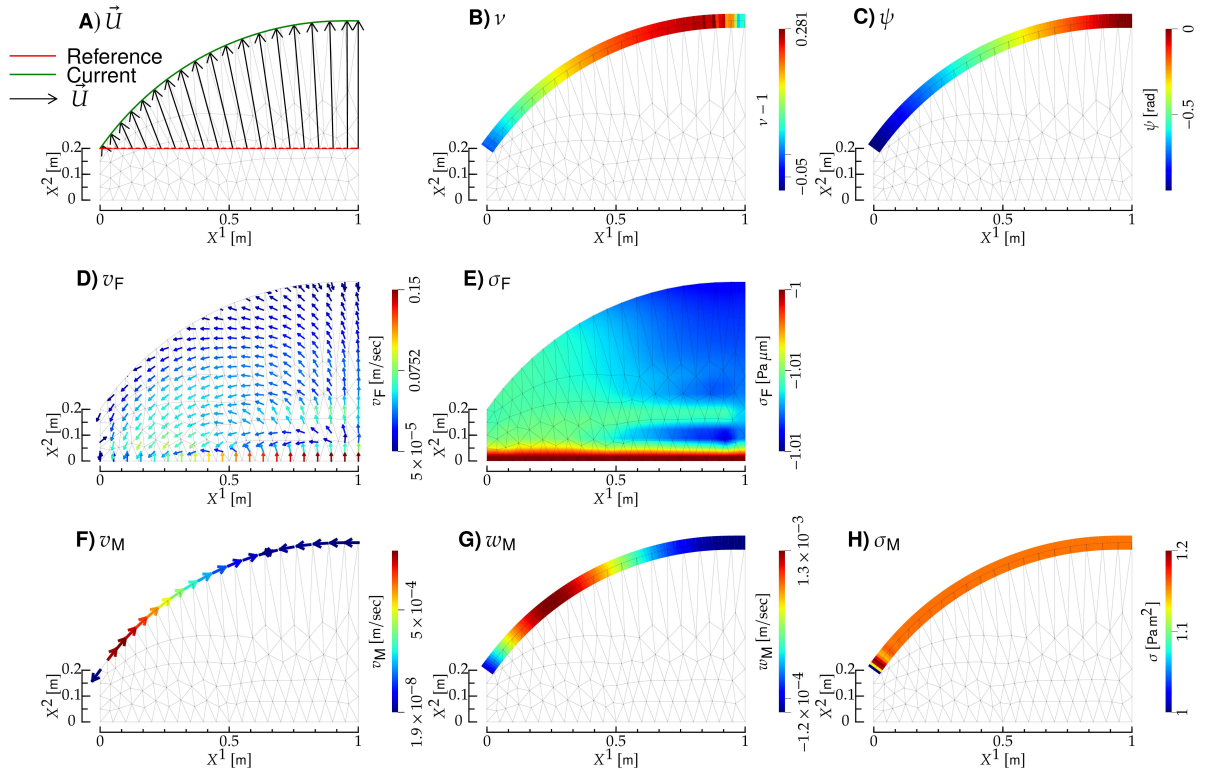


**FIG. 7:** Interaction between a bulk fluid and a Helfrich membrane. **A)** Membrane reference and current configuration (red and green curve, respectively), and displacement field (black arrows). **B)** Membrane stretch field. **C)** Membrane tangent angle. **D)** and **E)**) Bulk-fluid velocity and tension; the notation is the same as in Fig. 2. **F)**, **G)** and **H)**: membrane tangential velocity, normal velocity and tension; the notation is the same as in Fig. 6B, C and D, respectively. All panels refer to the same instant of time, shown on top, and display also the deformed mesh (gray lines).